ACS SENSORS

Article

Cite This: ACS Sens. 2019, 4, 1925−1933

pubs.acs.org/acssensors

A Fully Integrated and Self-Powered Smartwatch for Continuous Sweat Glucose Monitoring

Jiangqi Zhao,[†,‡,§,∥,#] Yuanjing Lin,[†,‡,§,⊥,#] Jingbo Wu,[†] Hnin Yin Yin Nyein,[†,‡,§] Mallika Bariya,[†,‡,§] Li-Chia Tai,[†,‡,§] Minghan Chao,[†] Wenbo Ji,[†,‡,§] George Zhang,[†,‡,§] Zhiyong Fan,[⊥] and Ali Javey*[,†,‡,§]

[†]Department of Electrical Engineering and Computer Sciences and [‡]Berkeley Sensor and Actuator Center, University of California, Berkeley, California 94720, United States

[§]Materials Sciences Division, Lawrence Berkeley National Laboratory, Berkeley, California 94720, United States

[∥]State Key Laboratory of Polymer Materials Engineering, Polymer Research Institute at Sichuan University, Chengdu 610065, China

[⊥]Department of Electronic and Computer Engineering, The Hong Kong University of Science and Technology, Clear Water Bay, Kowloon, Hong Kong SAR, China

Supporting Information

ABSTRACT: Wearable devices for health monitoring and fitness management have foreseen a rapidly expanding market, especially those for noninvasive and continuous measurements with real-time display that provide practical convenience and eliminated safety/infection risks. Herein, a self-powered and fully integrated smartwatch that consists of flexible photovoltaic cells and rechargeable batteries in the forms of a "watch strap", electrochemical glucose sensors, customized circuits, and display units integrated into a "dial" platform is successfully fabricated for real-time and continuous monitoring of sweat glucose levels. The functionality of the smartwatch, including sweat glucose sensing, signal processing, and display, can be supported with the harvested/converted solar energy without external charging devices. The Zn-MnO_2 batteries serve as intermediate energy storage units and the utilization of aqueous electrolytes eliminated safety concerns for batteries, which is critical for wearable devices. Such a wearable system in a smartwatch fashion realizes integration of energy modules with self-powered capability, electrochemical sensors for noninvasive glucose monitoring, and *in situ* and real-time signal processing/display in a single platform for the first time. The as-fabricated fully integrated and self-powered smartwatch also provides a promising protocol for statistical study and clinical investigation to reveal correlations between sweat compositions and human body dynamics.

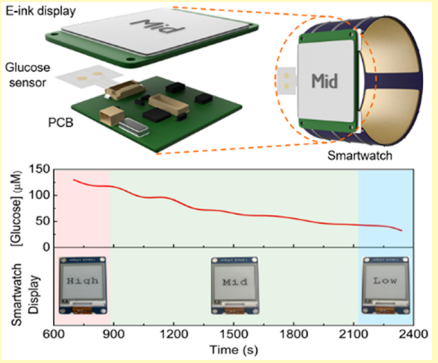

KEYWORDS: *flexible biosensors, noninvasive glucose monitoring, self-powered system, wearable electronics, healthcare and fitness management*

Wearable bioelectronics technology is a prominent research field owing to its promising applications toward personalized healthcare and fitness monitoring.[1−8] Among various bioelectronics, the development of sweat sensors has recently drawn considerable attention for its potential applications in point-of-care monitoring and health management in a continuous and noninvasive manner.[9−16] As a benefit of the easy access and rich composition, sweat offers great opportunities for real-time monitoring of an individual's health conditions at the molecular level.[1,2] Particularly, recent advancements in wearable devices based on sweat sensing have made it possible to noninvasively detect a variety of species, including electrolytes, metabolites, acids, heavy metals, and drugs, for applications in health monitoring and disease diagnosis.[9−18] However, there still exist several major challenges for the wide applications of wearable sensors. First, current wearable devices mainly rely on wireless data transmission (e.g., Bluetooth, Radio Frequency, Zigbee) and external display components (e.g., mobile phones, computers) to achieve real-time data analysis/feedback,[19−24] which largely limit the miniaturization of the entire setup. Moreover, these supporting components for data processing and display require power supply for operation. Currently, most of the built-in batteries for wearable devices are rigid, considerably bulky, and require external charging or frequent replacement.[1,11−13] Besides, the intrinsic safety issues for the commonly used batteries, lithium batteries, for example, have raised safety concerns for wearable devices.[25,26] Recently, the aqueous rechargeable zinc−manganese oxide (Zn−MnO_2) battery, with unique features such as improved safety, light weight, ecofriendliness, high output voltage, and high capacity, have become one of the most promising alternatives to conventional batteries.[25−28] Apart

Received: May 14, 2019
Accepted: June 25, 2019
Published: July 4, 2019

DOI: 10.1021/acssensors.9b00891
ACS Sens. 2019, 4, 1925−1933

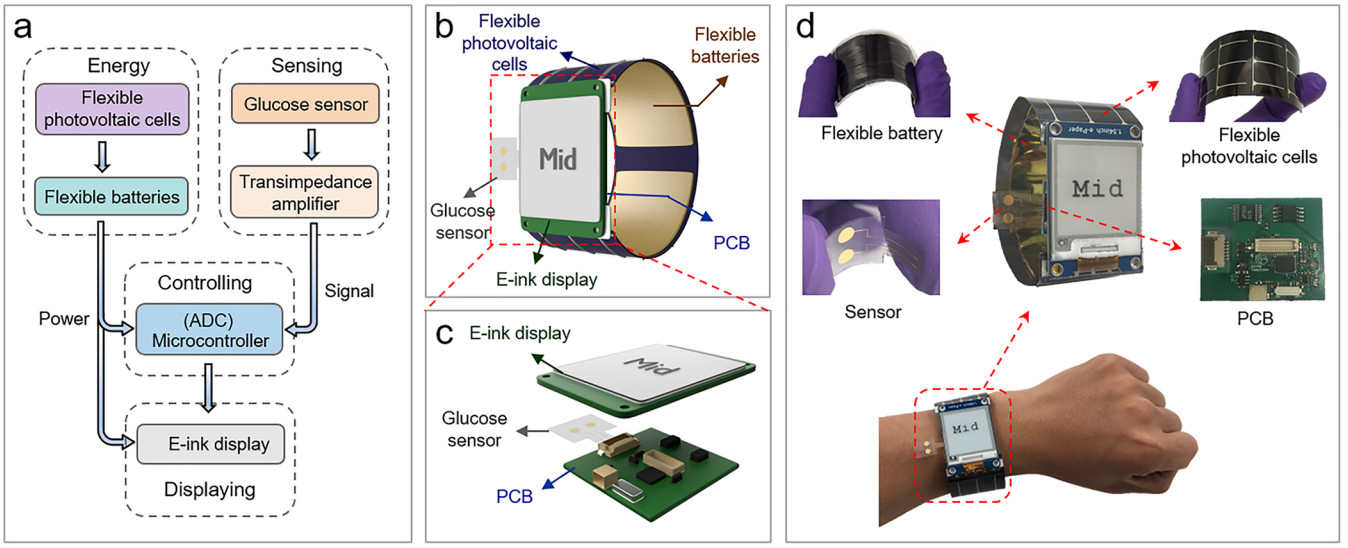

Figure 1. (a) System-level block diagram of the self-powered smartwatch. (b,c) Schematic illustrations of the self-powered smartwatch. (d) Images of the smartwatch on a subject's wrist and separate components.

from this, with the rapid advance of energy harvesting/conversion devices, the construction of a self-powered system that utilizes clean and sustainable energy from the surrounding environment (e.g., solar energy, mechanical vibrations and frictions, biofluids, etc.) to support the active device operation has raised intense research interest and is proposed to be one of the development directions for future wearable electronics.[29,30] However, due to the engineering complexity and the challenge of integrations, the construction of a fully integrated and self-powered system that enables real-time health monitoring/fitness management and *in situ* data analysis/display has not been reported.

Here, we report a fully integrated self-powered smartwatch for noninvasive and continuous monitoring of glucose levels. The smartwatch consists of flexible photovoltaic cells for energy harvesting and conversion, flexible Zn-MnO_2 rechargeable batteries as intermediate energy storage devices, an electrochemical sensor for sweat glucose monitoring, a printed circuit board (PCB) as controlling module, and electronic ink (E-ink) display to facilitate direct and real-time monitoring. In such a fully integrated system, the harvested/converted energy from amorphous silicon (a-Si) photovoltaic cells can be stored in the batteries and provide adequate power for the operation of the whole system, including real-time signal processing and data display, without external power sources. It is worth mentioning that the as-fabricated Zn-MnO_2 batteries based on quasi-solid-state aqueous electrolytes eliminate the safety concerns for batteries and deliver high energy storage capacity, long cycling lifetime, and desirable mechanical stability. Besides, the as-prepared glucose sensors demonstrate remarkable sensitivity and stability for reliable sweat glucose monitoring. In particular, due to the desirable flexibility of the power devices and sensors, the smartwatch can be comfortably worn on the wrist. On-body sweat glucose real-time and continuous monitoring was demonstrated with different sweat generation methods, including iontophoresis sweat extraction, and indoor and outdoor exercising. The presented fully integrated smartwatch realizes energy harvesting/storage, biosensing, signal processing, and display in a single platform to achieve a self-powered sweat glucose monitoring system, paving the way for daily healthcare and fitness management as well as various clinical research in a noninvasive fashion.

RESULTS AND DISCUSSION

The system-level overview of the sensing and power supply operation modes is shown in Figure 1a. The enzymatic sensor enables selective redox reaction with the glucose in the sweat secretion and generates output amperometric signals, which are amplified by a transimpedance amplifier (TIA) and further converted into the digital signals by an analog-to-digital (ADC) port within the microcontroller. Subsequently, the microcontroller analyzes these digital signals, filters out high-frequency noise, and transmits the processed results to an E-ink display for real-time *in situ* monitoring (a more detailed diagram is shown in Figure S1). The E-ink module provides the merits of stable display without a continuous power supply, ultralow power consumption, wide viewing angle, and high visibility and contrast. The harvested/converted energy from photovoltaic cells can support system operation, or can be stored in batteries and released to compensate for inadequate power supply with illuminance fluctuations. The protocol of the fully integrated and self-powered smartwatch for sweat glucose monitoring is schematically illustrated in Figure 1b with more technical details provided in the Experimental Section. The wristband of the as-assembled smartwatch served as the power supply module, consisting of two flexible photovoltaic cells connected in parallel facing outside for efficient energy harvesting, with three flexible batteries connected in series placed on the other side that can be charged up to 6.0 V. As shown in Figure 1c, the customized PCB (detailed layout design and information are shown in Figure S2) located under the E-ink display enables signal processing/filtering, sensor conditioning, and output display control. The sensors are fabricated on mechanically flexible polyethylene terephthalate (PET) substrates and can be directly inserted into the PCB through a connector (Figure 1c), which provides convenience for sensor replacement. The desirable flexibility of the as-assembled wearable smartwatch is demonstrated Figure 1d.

Rechargeable batteries as intermediate energy storage devices are essential for the continuous functionality of the smartwatch

DOI: 10.1021/acssensors.9b00891
ACS Sens. 2019, 4, 1925−1933

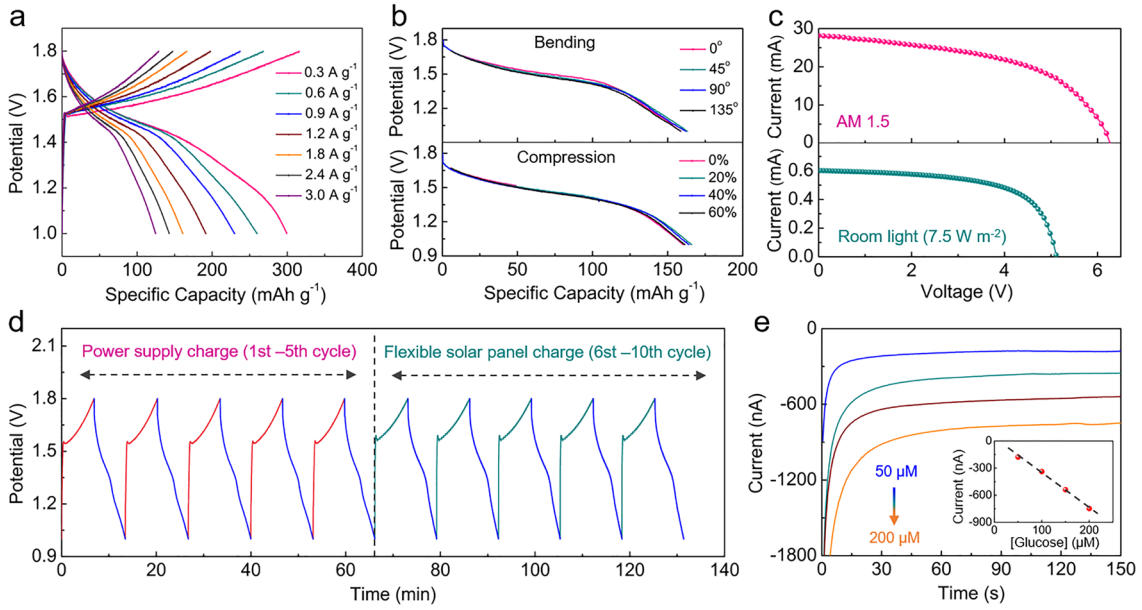

Figure 2. (a) Charge/discharge curves of the battery at different current densities. (b) Charge/discharge curves of the battery under different bending conditions (up) and different compression conditions (below). (c) Current–voltage (I–V) curve for the flexible photovoltaic cell under AM 1.5 (up) and room light (below). (d) Voltage–time (V–t) curves of the flexible photovoltaic cell–flexible battery device (during the first–fifth cycles: both galvanostatically charged and discharged at 1 mA using workstation; during the sixth–tenth cycles: charged at 1 mA using flexible photovoltaic cell and galvanostatically discharged at 1 mA using workstation). (e) Chronoamperometric responses of a glucose sensor.

even with inadequate power supply from photovoltaic cells. Zn-MnO_2 rechargeable batteries based on aqueous electrolyte with desirable operational safety have emerged as a promising alternative candidate to commercially available batteries that use flammable organic electrolytes.[31,32] The Zn-MnO_2 flexible batteries were fabricated by depositing MnO_2 and Zn onto porous nitrogen-doped carbon foams (N-CF) to serve as cathode and anode, respectively. The high porosities of the hydrothermal deposited MnO_2@N-CF cathodes and electroplated Zn@N-CF anodes are shown in scanning electron microscopy (SEM) images in Figure S3. The as-fabricated electrodes provide desirable mechanical flexibility for wearable devices, as well as high porosity and large specific surface areas to facilitate the electrolyte ion penetration and fast charge transport, which is critical to realize high energy storage capacity. PVA-based aqueous gel electrolyte consisting of $LiCl/ZnCl_2/MnSO_4$ was utilized to form the quasi-solid-state Zn-MnO_2 flexible batteries. The performance of the as-fabricated batteries was evaluated by cyclic voltammetry (CV) measurements and galvanostatic charge/discharge (GCD) tests. As shown in Figure S4, the CV curve of the flexible battery displays a reduction peak at 1.35 V and an oxidation peak at 1.66 V, which is consistent with the previous literature.[33]

Figure 2a presents the GCD curves of the Zn-MnO_2 flexible batteries at various charging/discharging current densities. The as-fabricated batteries yield a highest capacity of 301 mA h g^{-1} at 0.3 A g^{-1}, which is remarkably competitive compared to the reported values.[34−37] Besides, the capacity retained 125 mA h g^{-1} at a high current density of 3 A g^{-1}, which indicates a good rate capability and ultrafast charge–discharge ability. The excellent mechanical robustness of the batteries based on the N-CFs can be demonstrated with negligible decrease in capacities under bending and compression, as shown in Figure 2b. Furthermore, the battery retains 91.86% of the initial capacitance after 1000 cycles of charging/discharging at a high current density of 1.8 A g^{-1}, demonstrating excellent cyclic stability (Figure S5). Such remarkable energy storage capacity and mechanical stability endows the as-fabricated flexible battery with great feasibility in flexible and wearable applications.

The as-fabricated rechargeable Zn-MnO_2 batteries can be properly charged with the energy harvested and converted by photovoltaic cells, thus realizing the self-powered functionality. As shown in Figure 2c, the flexible photovoltaic cells with device area around 28.44 cm^2 used in the smartwatch can generate a short-circuit photocurrent (I_{sc}) of 28.79 mA and an open-circuit voltage (V_{oc}) of over 6.28 V, with a power-conversion efficiency (PCE) of 3.20%, under air mass (AM) of 1.5. Under the relatively low intensity of room light (around 7.5 W m^{-2}), the I_{sc} and V_{oc} are 0.6 mA and 5.12 V, respectively, with a PCE of 9.04%. In general, the a-Si photovoltaic cells delivered a relatively higher PCE under lower light intensities as shown in Figure S6. The photocharging properties were demonstrated with an integrated self-powered module that consists of two photovoltaic cells connected in parallel and one Zn-MnO_2 battery with a photocharging current and galvanostatic discharging current around 1 mA, as shown in Figure 2d. The as-obtained GCD curves of the battery with photocharging are stable over all the cycles and delivered similar performance compared with those under standard GCD measurements, indicating the excellent properties of the integrated photocharging self-powered energy source.[38]

As a functional demonstration, flexible electrochemical sensors for noninvasive glucose monitoring were integrated into the system. The sensors are in two-electrode configuration and are composed of an enzyme-based glucose electrode as working electrode and an Ag/AgCl electrode serving as counter electrode. The performance of glucose sensors was characterized in glucose solutions with concentrations ranging from 50 to 200 μM (typical glucose concentrations in human sweat), and the chronoamperometric responses are shown in Figure 2e. A linear relationship between output currents and glucose concen-

DOI: 10.1021/acssensors.9b00891
ACS Sens. 2019, 4, 1925−1933

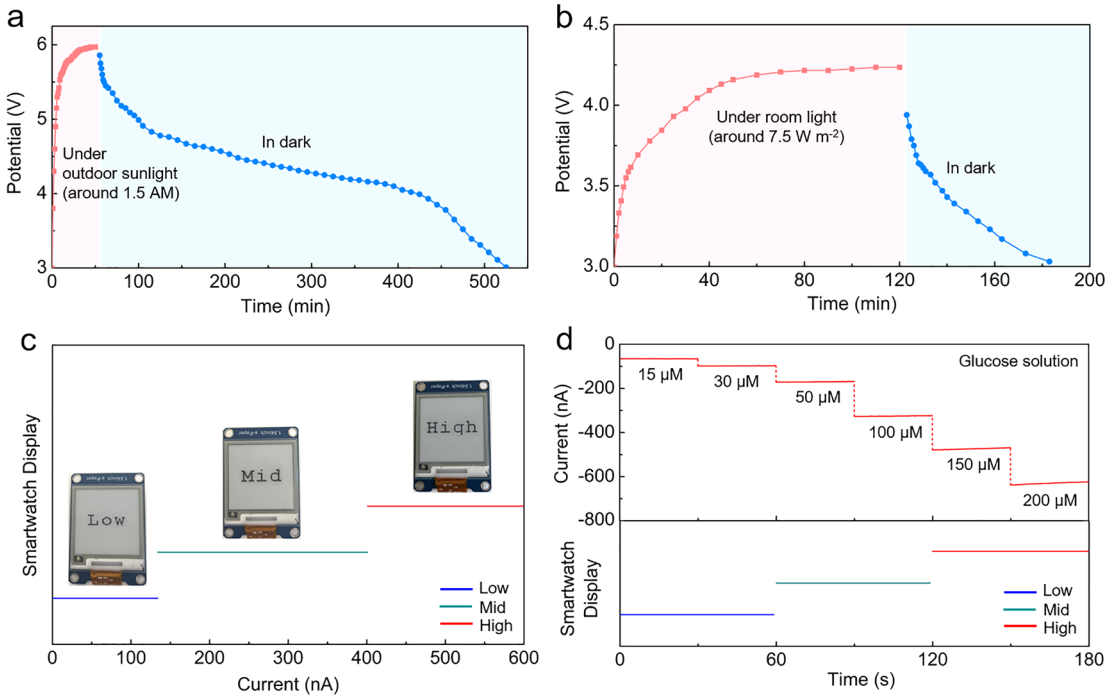

Figure 3. Charging and discharging curves of the smartwatch under (a) outdoor sunlight and (b) room light. (c) Displays of the smartwatch corresponding to different current ranges. (d) Chronoamperometric responses of a sensor to glucose solutions in different concentrations (up) and the corresponding smartwatch display (below).

trations was observed. Reproducibility of the sensors is presented in Figure S7a, showing an average sensitivity of 3.29 nA μM^{-1}, with a relative standard deviation (RSD) of 8.8%. The average sensitivity was later used as a standard calibration value for sweat glucose monitoring. Long-term continuous measurement shows that the sensors maintained a sensitivity of 3.18 nA μM^{-1} after 2 h long-term measurements (Figure S8), which is within a variation of 3.3% compared to the average sensitivities of the as-fabricated sensors. Moreover, since sweat normally contains a wide variety of chemicals that can potentially interfere with the glucose detection, the selectivity of sweat sensors is also a crucial factor. The as-fabricated glucose sensors delivered good selectivity for glucose sensing in the presence of other biomolecules (including lactate, ascorbic acid, uric acid, and NaCl), as shown in Figure S7b. Furthermore, after 30 cycles of bending and 30 instances of skin contact/friction, the sensors retained the average sensitivities of 3.08 and 3.10 nA μM^{-1} (with variations of 6.4% and 5.8%), respectively (Figure S9), which are within the error range. The results demonstrated desirable stability under mechanical deformation, skin contact, and friction, which is essential for on-body monitoring.

With systematic performance characterization and dedicated system design for operation parameters matching among energy harvesting and storage devices, glucose sensors, and output signal processing/display, a fully integrated self-powered smartwatch for glucose monitoring was then successfully assembled. The power supply module of the smartwatch consists of two photovoltaic cells connected in parellel and three Zn-MnO_2 batteries connected in series. The integrated self-powered smartwatch can be charged up to 6.0 V within 1 h under outdoor sunlight (approximately AM 1.5), which shows a desirable quick charging capability. With the solar energy stored in the batteries, the system achieves a cruising duration of up to 8 h with a cutoff potential of 3 V, as shown in Figure 3a. It is also worth mentioning that by utilizing aqueous electrolyte, a desirable operational safety can be realized. Compared with batteries based on flammable organic electrolytes, it eliminates the safety concerns under increasing cell temperatures, especially with relatively large heat generation under outdoor charging. Under relatively low illuminance under room light (around 7.5 W m^{-2}), it takes around 2 h to charge the integrated self-powered device to 4.2 V, and the stored energy in the batteries can support system functions for around 1 h (Figure 3b), delivering an energy transfer efficiency of 33% from solar cell to battery. These results demonstrate that the as-fabricated fully integrated system realize a self-powered property without external power sources and can achieve reliable performance in both indoor and outdoor environments, even with interruption from insufficient illumination.

Maintaining a glucose level in the normal range is critical for health management, while both high and low levels of glucose might indicate a risk of metabolic disorders, such as diabetes or hypoglycemic shock, especially after intense exercise. To realize the convenient analysis of sweat glucose level by users, the smartwatch display is designed to provide alarm signals from "low", "medium", to "high" according to the output currents of the sensors, instead of displaying the glucose concentration values. The current detection resolution of the smartwatch based on the customized circuit can reach 6 nA, corresponding to a glucose concentration of around 2 μM. Referring to previously reports on sweat glucose monitoring, the glucose concentrations of 40 μM and 120 μM were set as threshold values for E-ink display to switch the glucose level alarm from low to medium and medium to high, respectively (Figure 3c).[1,3,7,8,19] Figure 3d shows the representative current responses of the glucose sensors and the corresponding alarm signals on E-ink display. The glucose level was indicated as "Low" in both 15 μM and 30 μM glucose solutions with the sensor output currents of 63 nA and 98 nA, respectively. When the glucose concentrations were increased to 50 μM (169 nA)

DOI: 10.1021/acssensors.9b00891
ACS Sens. 2019, 4, 1925−1933

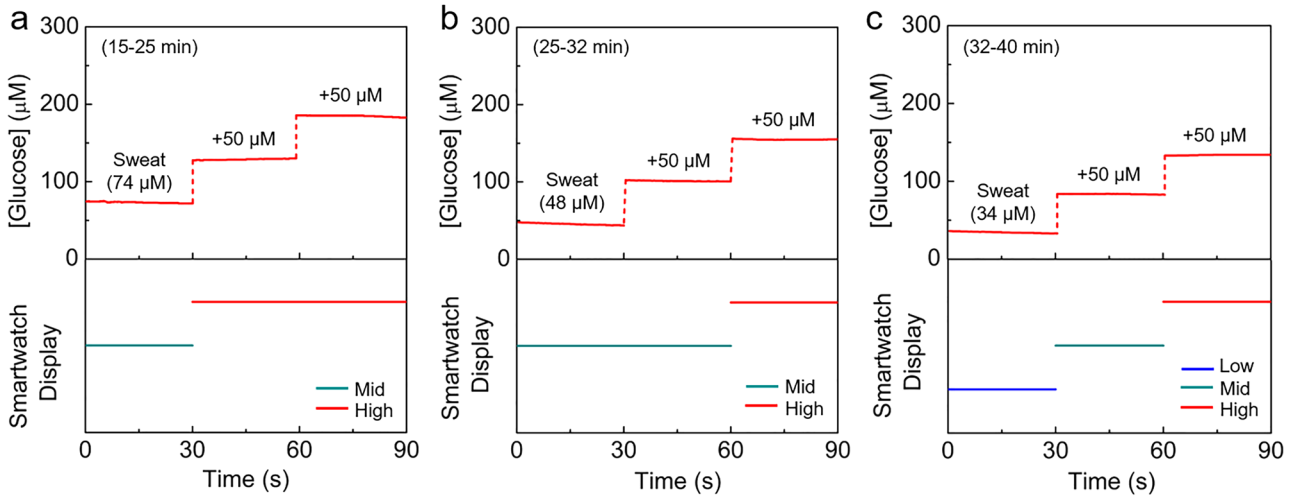

Figure 4. Verification of the accuracy of sweat glucose level monitoring by smartwatch based on exercise induced sweat samples during different time ranges. The displayed sweat glucose level (bottom) matched the sweat glucose concentration changes (top) well.

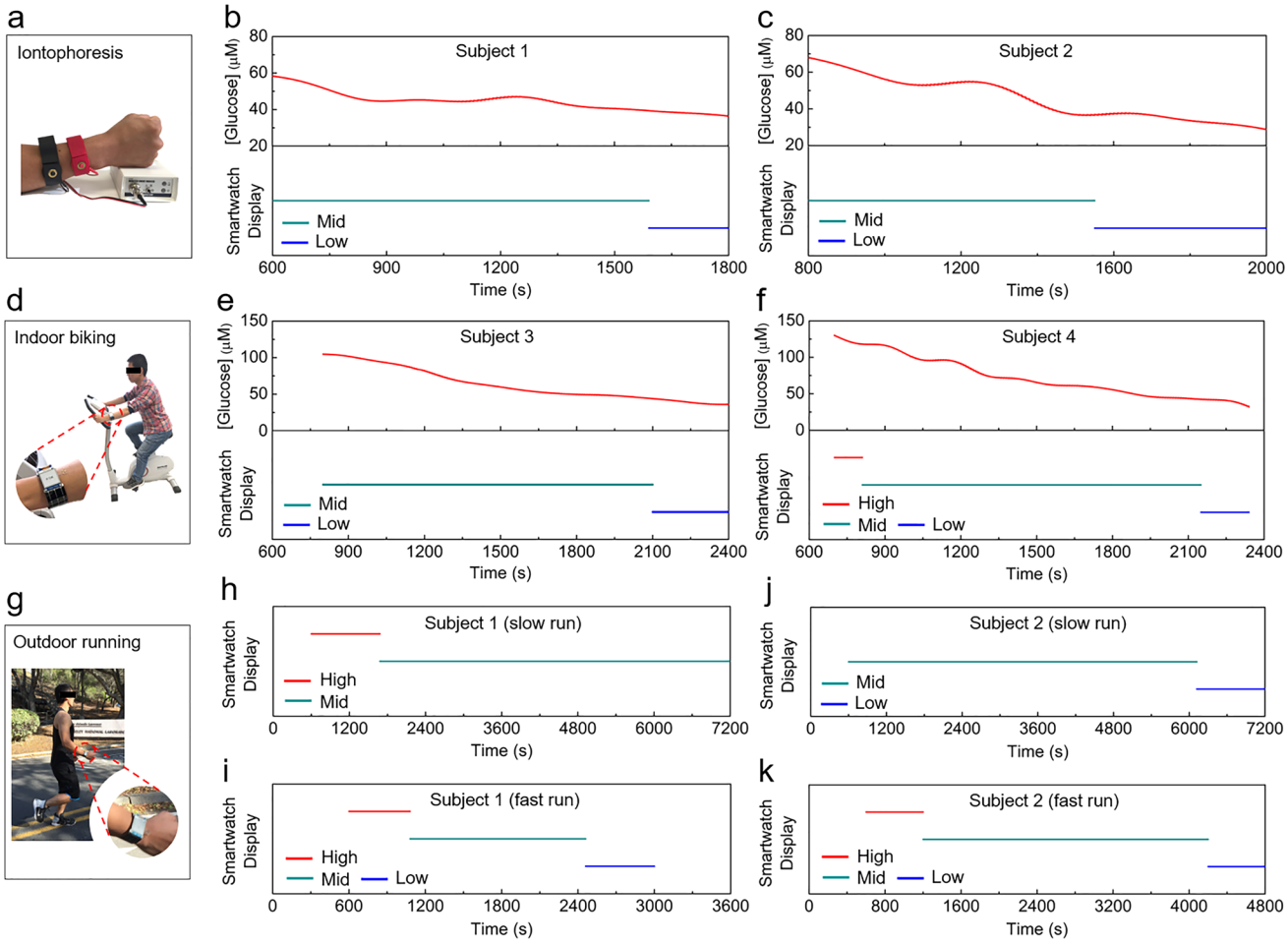

Figure 5. (a) Image of iontophoresis-based sweat extraction. (b,c) Real-time measurements of sweat glucose level for subjects during equilibrium status. (d) A smartwatch is worn on a subject's wrist during indoor biking. (e,f) Dynamic changes of sweat glucose level during cycling. (g) A smartwatch is worn on a subject's wrist during outdoor running. Dynamic changes of sweat glucose level during slow run (h,i) and fast run (j,k).

and 100 μM (324 nA), the display changed to "Mid". An alarm signal of "High" glucose concentrations will be presented with concentrations of 150 μM (470 nA). Thus, the concentration range of glucose can be directly displayed for convenient analysis.

The accuracy of the displayed glucose level with the as-fabricated self-powered smartwatch was carefully verified with sweat samples collected from subjects during ergometer-based cycling exercise. Glucose standard solutions were subsequently added into the original sweat samples and characterized with the

DOI: 10.1021/acssensors.9b00891
ACS Sens. 2019, 4, 1925−1933

smartwatch and electrochemical workstation, respectively. Meanwhile, the initial glucose concentrations of the original sweat samples can be back-calculated based on the output currents of the sensors. As shown in Figure 4a, the glucose concentration in the sweat sample collected in the time range of 15−25 min during exercise is calculated to be 74 μM, at which point the smartwatch indicated a medium sweat glucose level ("Mid"). The display of the smartwatch changes to "High" with the concentration increased by 50 μM. After 32 min of exercise, the glucose concentration in the collected sweat sample decreased to 34 μM, and the smartwatch displays "Low", correspondingly (Figure 4c). Such a tendency to decrease is consistent with our previous study[1] and the reliability of glucose level monitoring with the smartwatch is well demonstrated.

The stable functionality of the fully integrated and self-powered smartwatch was further demonstrated via on-body evaluations based on various sweat extraction modes. To verify the accuracy of signal processing of the smartwatch, an extra glucose sensor was located within the same sweat extraction area and the output current can be read out with a workstation. Thus, the display glucose level can be compared with the output currents for verification. As shown in Figure 5a, iontophoresis (a sweat inducing technique) was utilized for sweat extraction, to evaluate the changes of glucose levels at equilibrium states. As shown in Figure 5b and c, the initial glucose concentrations in sweat were around 50 μM (E-ink display showed "Mid") for both two subjects, and slowly decreased to approximately 40 μM afterward with the displayed information changing to "Low" accordingly. Apart from sweat glucose monitoring during equilibrium status, real-time glucose monitoring during dynamic activities is also significant for fitness management. Figure 5d shows the image of a subject wearing the self-powered smartwatch during indoor cycling. Figure 5e,f depicts a real-time sweat glucose profile with exercise time. It is worth mentioning that without an adequate amount of sweat extracted in the first 10 min,[11] the output signals are unstable and unreliable. Therefore, the monitoring was triggered after 10 min of warming, and the as-detected glucose levels slowly decrease during continuous biking at a power of 150 W, which are similar to our previous study results.[11] The dynamic changes of glucose levels at different exercise intensities was also investigated during outdoor running at different speeds (Figure 5g). It is observed that the glucose levels drop below the set point after 2 h running at a slower running rate (~5 km h^{-1}) (Figure 5h and i), while at a faster running rate (~10 km h^{-1}), the glucose levels significant decreased in a shorter period of time (Figure 5j and k). The glucose levels indicated on the smartwatch delivered high consistency with the detection values via the workstation, which demonstrated the operational reliability of the smartwatch and its great promise for daily glucose level monitoring as well as fitness management. However, intensive research efforts are still required to reveal the correlations between sweat glucose level and blood glucose. In this work, sweat glucose sensing is adopted as a functional demonstration of the self-powered smartwatch, which can also be conveniently modified for biosensing with a variety of analytes.

CONCLUSION

For the first time, we have successfully demonstrated a fully integrated and self-powered wearable system in a smartwatch fashion for continuous monitoring of sweat glucose levels. Without external charging facilities, the smartwatch can be self-powered with flexible photovoltaic cells for energy harvesting/conversion and flexible Zn-MnO_2 batteries as energy storage devices. Such photocharging batteries performed a stable self-powered capability with a high energy storage capacity to support the continuous functionality of the system. The glucose sensors delivered desirable sensitivity and selectivity for sweat glucose monitoring and the integrated PCB and E-ink screen enables real-time and *in situ* data analysis/display, which eliminates transmission units and external reading devices. Such fully integrated systems provide operational convenience and safety, as well as device miniaturization, which are highly desirable for wearable and portable applications. Notably, the reliability of such a self-powered smartwatch for real-time glucose level monitoring was verified. Real-time and continuous on-body evaluation on sweat glucose level with the as-fabricated smartwatch was successfully conducted during both equilibrium status and dynamic activities. The as-developed fully integrated and self-powered smartwatch is highly desirable in daily health monitoring and fitness management, and provides a promising protocol for statistical studies to reveal correlations between sweat compositions and human body dynamics.

EXPERIMENTAL SECTION

Materials and Supporting Electronics. Zinc sulfate heptahydrate ($ZnSO_4{\cdot}7H_2O$), zinc chloride ($ZnCl_2$), manganese acetate [$Mn(CH_3COO)_2{\cdot}4H_2O$], isopropyl alcohol (IPA), polyvinyl chloride (PVC), manganese sulfate ($MnSO_4$), sodium sulfate (Na_2SO_4), potassium ferricyanide [$K_3(Fe(CN)_6)$], iron(III) chloride ($FeCl_3$), hydrochloric acid (HCl), chitosan, and glucose enzyme were obtained from Sigma-Aldrich. Commercial melamine sponge was obtained from Oh My Clean (Carpinteria, CA). All reagents were used as received. The commercial flexible photovoltaic cells (LL200−4.8−37) based on amorphous silicon were obtained from PowerFilm Inc. (Ames, IA).

Fabrication and Characterizations of Zn-MnO_2 Batteries. First, nitrogen-doped carbon foams (N-CFs) were prepared by pyrolyzing commercial melamine sponges at 800 °C under nirogen (N_2) atmosphere and used as free-standing current collectors for batteries. The pretreated N-CFs were then immersed in a 2 mM $KMnO_4$ aqueous solution and kept in an oven at 60 °C for 24 h to obtain MnO_2@N-CF cathodes. Zn@N-CF anodes were prepared by depositing Zn onto N-CF at a constant voltage of −1.5 V for 10 min in a mixing solution of 0.1 M $ZnSO_4$ and 0.1 M $NaSO_4$. A separator (NKK separator, Nippon Kodoshi Corporation) with PVA-based electrolyte was sandwiched between the as-fabricated MnO_2@N-CF cathode and Zn@N-CF anode to realize a quasi-solid-state flexible Zn-MnO_2 battery. The electrolyte gel was prepared by mixing 3 M LiCl, 2 M $ZnCl_2$, 0.1 M $MnSO_4$, and PVA (0.1 g mL^{-1}) in deionized (DI) water and heated at 85 °C for 2 h under vigorous stirring. The morphologies of the as-fabricated electrodes were analyzed using SEM (Quanta 3D FEG, FEI). Electrochemical performances of the batteries were characterized based on galvanostatic testing in the voltage range of 1.0−1.8 V using a Land 2001A battery testing system (Wuhan, China). E-Ink Display Module (1.54 in.) was obtained from Waveshare Electronics (Shenzhen, China).

Fabrication and Characterization of Glucose Sensors. The glucose sensors were fabricated on flexible PET substrates in two-electrode configuration, which is a common strategy for low current electrochemical sensors.[1] The PET substrates were first cleaned with IPA and O_2 plasma etching. Afterward, a pair of electrodes with a diameter of 3 mm were patterned via photolithography and thermally evaporated with 30/50 nm of Cr/Au, followed by lift-off in acetone. Then, a layer of Ag/AgCl paste was applied evenly on one of the as-fabricated Au electrodes and dried at 120 °C, which serves as the reference/counter electrode for the glucose sensor. For working electrode, a Prussian blue mediator layer was first deposited onto the Au electrode by cyclic voltammetry from 0 to 0.5 V (versus Ag/AgCl) for one cycle at a scan rate of 20 mV s^{-1} in a fresh solution containing 2.5 mM $FeCl_3$, 100 mM KCl, 2.5 mM $K_3Fe(CN)_6$, and 100 mM HCl.

DOI: 10.1021/acssensors.9b00891
ACS Sens. 2019, 4, 1925−1933

Then, a nickel hexacyanoferrate (NiHCF) layer was deposited via CV scanning deposition with a potential window of 0−0.8 V at a scan rate of 100 mV s^{-1} for 10 cycles in a electrolyte containing 0.5 mM $K_3Fe(CN)_6$, 0.5 mM $NiCl_2$, 0.1 M HCl, and 0.1 M KCl. The enzyme membrane solution was obtained by mixing agarose solution (1 wt %) with glucose oxidase solution (1 mg of enzyme in 100 μL of PBS with a pH value of 7.2) in a 1:1 v/v ratio. Then, 4 μL of the membrane solution was cast over the working electrode and allowed to dry overnight at ambient temperature. The obtained glucose sensors were first characterized chronoamperometrically based on a three-electrode configuration using workstation (CHI 1230C) before being applied to an on-body test.

PCB Design. The entire circuit was based around the Tinyduino microcontroller (TinyCircuits) (Akron, OH) with accompanying analog circuitry for signal conditioning, processing, and controlling e-ink display. For the signal conditioning block, TLE2426 virtual ground (Texas Instruments) (Dallas, TX) was used for producing a reference voltage level for DPV. LTC6079 amplifier was chosen accompanied by a resistor to make a trans-impedance amplifier to convert the sensor's current signal into a voltage signal. After this, the voltage signal is fed into an Atmega328p (Atmel 8-bit) (Microchip Technology) (Chandler, AZ) microcontroller's ADC. The preprogramed Infinite impulse response (IIR) low-pass filter will de-noise the signal (Figure S2, the signal condition diagram) and the processed signal will be used as a reference for display. The microcontroller communicates with E-Ink module via Serial Peripheral Interface (SPI) and it can be programmed on-board by Alf and Vegard's Reduced Instruction Set Computer (AVR-RISC) programmer or Universal Serial Bus (USB) after burning a bootloader into it.

Off-Body Evaluation of Sweat Samples. The subjects performed cycling exercise on a stationary ergometer (Kettler E3 Upright Exercise Bike) with 150 W power output. Once the subjects started sweating, sweat samples were collected every 5 min using centrifuge tubes from the foreheads of the subjects. After each collection, the subjects cleaned their foreheads with gauze. The sweat samples were initially evaluated using a workstation (CHI 1230C) and the integrated wristband, respectively. Then, standard glucose solutions were added into the sweat samples and the output current and E-ink display data were recorded. The initial glucose concentrations in the sweat samples were back-calculated based on the change in output currents with concentration variations.

On-Body Sweat Glucose Analysis Using the Integrated Wristband. The on-body sweat glucose monitoring was demonstrated with the integrated wristband in compliance with the protocol that was approved by the institutional review board at the University of California, Berkeley (CPHS 2014-08-6636 and CPHS 2015-05-7578). Six healthy male subjects, aged 20−30, were recruited from the University of California, Berkeley campus, and all subjects gave written, informed consent before participating in the study. For the on-body test, the subjects' wrists were first cleaned with alcohol swabs (BD Inc. NJ, USA). After that, a 1 × 1 cm^2 water-absorbent thin rayon pad (TX609, Texwipe, USA) was sandwiched between the skin and the sensor to absorb and maintain sufficient sweat for stable and reliable sensor readings. The pad could absorb about 10 μL of sweat, which was sufficient to provide stable sensor readings. In addition, a 4 × 6 cm^2 medical tape (ARcare 93690, Adhesives Research Inc., USA) was used to secure the sensor onto the skin and ensure good contact. A small hole (~1 mm in diameter) was punched into the substrate of the sensor for sweat flow. During on-body tests, the newly generated sweat would refill the pad and rinse away the old sweat through the hole. The study was conducted as three trials: iontophoresis sweat extraction, indoor biking, and outdoor running. For iontophoresis sweat extraction, pilocarpine hydrogel (ELITechGroup SS-023 Pilogel Discs) was first placed underneath the anode and cathode electrodes followed by applying a 1 mA DC current for 5 min to drive the pilocarpine into the subdermal regions of a subject to stimulate sweat glands (ELITechGroup Model 3700 Webster Sweat Inducer). Afterward, two glucose sensors were put on the sweat extraction area. One of the sensors was integrated into the wristband to get real-time output current data and the other one was connected to the workstation to verify the accuracy of obtained data from the integrated wristband. For indoor biking, Subjects were told to bike for 40 min on an electronically braked leg-cycle ergometer (Kettler E3 Upright Ergometer Exercise Bike). Cycling protocol included a 5 min ramp-up and a constant 35 min biking at a power of 150 W. Two glucose sensors were attached on the subject's wrist and connected with both wristband and workstation for data recording, respectively. For outdoor running, subjects wore the integrated wristband to run at different speeds (slow run: ~5 km h^{-1}, fast run: ~10 km h^{-1}), and the output data were recorded every minute.

Calculations. The energy-conversion efficiency of the flexible photovoltaic cells (η_1) was calculated from eq 1) as follows:[38]

$$\eta_1 = V_{oc} \times I_{sc} \times FF/(P \times S) \times 100\% \quad (1)$$

where FF, V_{oc}, I_{sc}, S, and P are fill factor, open-circuit voltage (V), short-circuit current (mA), effective area of cells (cm^{-2}), and incident light power density (100 mW cm^{-2}).

The energy transfer efficiency from solar cells to battery (η_2) was calculated from eq 2):[38]

$$\eta_2 = E_d/(P \times S \times t \times \eta_1) \times 100\% \quad (2)$$

where E_d and t are the discharge energy of battery (mWh) and photocharge time (h), respectively.

■ ASSOCIATED CONTENT

Supporting Information

The Supporting Information is available free of charge on the ACS Publications website at DOI: 10.1021/acssensors.9b00891.

Schematic diagram of signal-conditioning circuit; Images of PCB layout design; SEM images of the battery electrodes; CV curve, cycling performance, and coulombic efficiency; current-voltage curve; reproducibility and selectivity glucose sensor; long-term stability testing and responses of the glucose sensors (PDF)

■ AUTHOR INFORMATION

Corresponding Author

*E-mail: ajavey@berkeley.edu.

ORCID

Yuanjing Lin: 0000-0002-8568-1786
Hnin Yin Yin Nyein: 0000-0002-5692-6182
Mallika Bariya: 0000-0002-3416-8157
Wenbo Ji: 0000-0002-7913-361X
Zhiyong Fan: 0000-0002-5397-0129
Ali Javey: 0000-0001-7214-7931

Author Contributions

#J. Zhao and Y. Lin contributed equally to this work.

Notes

The authors declare no competing financial interest.

■ ACKNOWLEDGMENTS

The authors thank Dr. Mark Hettick, Dr. Chaoliang Tan, and Dr. Yingbo Zhao for their support on materials characterization. This work was supported by the National Science Foundation (NSF) Nanomanufacturing Systems for Mobile Computing and Mobile Energy Technologies (NASCENT), Berkeley Sensor and Actuator Center (BSAC), and Bakar fellowship.

■ REFERENCES

(1) Gao, W.; Emaminejad, S.; Nyein, H. Y. Y.; Challa, S.; Chen, K.; Peck, A.; Fahad, H. M.; Ota, H.; Shiraki, H.; Kiriya, d.; Lien, D. H.; Brooks, G. A.; Davis, R. W.; Javey, A. Fully integrated wearable sensor

DOI: 10.1021/acssensors.9b00891
ACS Sens. 2019, 4, 1925−1933

arrays for multiplexed in situ perspiration analysis. *Nature* **2016**, *529*, 509−514.
(2) Emaminejad, S.; Gao, W.; Wu, E.; Davies, Z. A.; Nyein, H. Y. Y.; Challa, S.; Ryan, S. P.; Fahad, H. M.; Chen, K.; Shahpar, Z.; Talebi, S.; Milla, C.; Javey, A. Autonomous sweat extraction and analysis applied to cystic fibrosis and glucose monitoring using a fully integrated wearable platform. *Proc. Natl. Acad. Sci. U. S. A.* **2017**, *114*, 4625−4630.
(3) Lee, H.; Choi, T. K.; Lee, Y. B.; Cho, H. R.; Ghaffari, R.; Wang, L.; Choi, H. J.; Chung, T. D.; Lu, N.; Hyeon, T.; Choi, S. H.; Kim, D.-H. A graphene-based electrochemical device with thermoresponsive microneedles for diabetes monitoring and therapy. *Nat. Nanotechnol.* **2016**, *11*, 566−572.
(4) Lee, H.; Song, C.; Hong, Y. S.; Kim, M. S.; Cho, H. R.; Kang, T.; Shin, K.; Choi, H. J.; Hyeon, T.; Kim, D. H. Wearable/disposable sweat-based glucose monitoring device with multistage transdermal drug delivery module. *Sci. Adv.* **2017**, *3*, No. e1601314.
(5) Chen, Y.; Lu, S.; Zhang, S.; Li, Y.; Qu, Z.; Chen, Y.; Lu, B.; Wang, X.; Feng, X. Skin-like biosensor system via electrochemical channels for noninvasive blood glucose monitoring. *Sci. Adv.* **2017**, *3*, No. e1701629.
(6) Koh, A.; Kang, D.; Xue, Y.; Lee, S.; Pielak, R. M.; Kim, J.; Hwang, T.; Min, S.; Banks, A.; Bastien, P.; Manco, M. C.; Wang, L.; Ammann, K. R.; Jang, K.-I.; Won, P.; Han, S.; Ghaffari, R.; Paik, U.; Slepian, M. J.; Balooch, G.; Huang, Y.; Rogers, J. A. A soft, wearable microfluidic device for the capture, storage, and colorimetric sensing of sweat. *Sci. Transl. Med.* **2016**, *8*, No. 366ra165.
(7) Kim, J.; Campbell, A. S.; Wang, J. Wearable non-invasive epidermal glucose sensors: A review. *Talanta* **2018**, *177*, 163−170.
(8) Bariya, M.; Nyein, H. Y. Y.; Javey, A. Wearable sweat sensors. *Nat. Electron.* **2018**, *1*, 160.
(9) McCaul, M.; Porter, A.; Barrett, R.; White, P.; Stroiescu, F.; Wallace, G.; Diamond, D. Wearable Platform for Real-time Monitoring of Sodium in Sweat. *ChemPhysChem* **2018**, *19*, 1531−536.
(10) Shiwaku, R.; Matsui, H.; Nagamine, K.; Uematsu, M.; Mano, T.; Maruyama, Y.; Nomura, A.; Tsuchiya, K.; Hayasaka, K.; Takeda, Y.; Fukuda, T.; Kumaki, D.; Tokito, S. A Printed Organic Circuit System for Wearable Amperometric Electrochemical Sensors. *Sci. Rep.* **2018**, *8*, 6368.
(11) Nyein, H. Y. Y.; Gao, W.; Shahpar, Z.; Emaminejad, S.; Chall, S.; Chen, K.; Fahad, H. M.; Tai, L.-C.; Ota, H.; Davis, R. W.; Javey, A. A Wearable Electrochemical Platform for Noninvasive Simultaneous Monitoring of Ca^{2+} and pH. *ACS Nano* **2016**, *10*, 7216−7224.
(12) Gao, W.; Nyein, H. Y. Y.; Shahpar, Z.; Fahad, H. M.; Chen, K.; Emaminejad, S.; Gao, Y.; Tai, L.-C.; Ota, H.; Wu, E.; Bullock, J.; Zeng, Y.; Lien, D.-H.; Javey, A. Wearable Microsensor Array for Multiplexed Heavy Metal Monitoring of Body Fluids. *ACS Sens.* **2016**, *1*, 866−874.
(13) Tai, L.-C.; Gao, W.; Chao, M.; Bariya, M.; Ngo, Q. P.; Shahpar, Z.; Nyein, H. Y. Y.; Park, H.; Sun, J.; Jung, Y.; Wu, E.; Fahad, H. M.; Lien, D.-H.; Ota, H.; Cho, G.; Javey, A. Methylxanthine Drug Monitoring with Wearable Sweat Sensors. *Adv. Mater.* **2018**, *30*, 1707442.
(14) Mohamed, M. A.; Fayed, A. S.; Hegazy, M. A.; Salama, N. N.; Abbas, E. E. Fully optimized new sensitive electrochemical sensing platform for the selective determination of antiepileptic drug ezogabine. *Microchem. J.* **2019**, *144*, 130−138.
(15) Imani, S.; Bandodkar, A. J.; Mohan, A. V.; Kumar, R.; Yu, S.; Wang, J.; Mercier, P. P. A wearable chemical-electrophysiological hybrid biosensing system for real-time health and fitness monitoring. *Nat. Commun.* **2016**, *7*, 11650.
(16) Selvam, A. P.; Muthukumar, S.; Kamakoti, V.; Prasad, S. A wearable biochemical sensor for monitoring alcohol consumption lifestyle through Ethyl glucuronide (EtG) detection in human sweat. *Sci. Rep.* **2016**, *6*, 23111.
(17) Joseph, J. I.; Torjman, M. C.; Strasma, P. J. Vascular glucose sensor symposium: continuous glucose monitoring systems (CGMS) for hospitalized and ambulatory patients at risk for hyperglycemia, hypoglycemia, and glycemic variability. *J. Diabetes Sci. Technol.* **2015**, *9*, 725−738.
(18) Abellán-Llobregat, A.; Jeerapan, I.; Bandodkar, A.; Vidal, L.; Canals, A.; Wang, J.; Morallon, E. A stretchable and screen-printed electrochemical sensor for glucose determination in human perspiration. *Biosens. Bioelectron.* **2017**, *91*, 885−891.
(19) Lee, H.; Hong, Y. J.; Baik, S.; Hyeon, T.; Kim, D. H. Enzyme-based glucose sensor: from invasive to wearable device. *Adv. Healthcare Mater.* **2018**, *7*, 1701150.
(20) Hong, Y. J.; Lee, H.; Kim, J.; Lee, M.; Choi, H. J.; Hyeon, T.; Kim, D. H. Multifunctional Wearable System that Integrates Sweat-Based Sensing and Vital-Sign Monitoring to Estimate Pre-/Post-Exercise Glucose Levels. *Adv. Funct. Mater.* **2018**, *28*, 1805754.
(21) Kim, J.; Jeerapan, I.; Imani, S.; Cho, T. N.; Bandodkar, A.; Cinti, S.; Wang, J. Noninvasive alcohol monitoring using a wearable tattoo-based iontophoretic-biosensing system. *Acs Sens.* **2016**, *1*, 1011−81019.
(22) Sekine, Y.; Kim, S. B.; Zhang, Y.; Bandodkar, A. J.; Xu, S.; Choi, J.; Irie, M.; Ray, T. R.; Kohli, P.; Kozai, N.; Sugita, T.; Wu, Y.; Lee, K.; Lee, K.-T.; Ghaffari, R.; Rogers, J. A. A fluorometric skin-interfaced microfluidic device and smartphone imaging module for in situ quantitative analysis of sweat chemistry. *Lab Chip* **2018**, *18*, 2178−2186.
(23) Bandodkar, A. J.; Gutruf, P.; Choi, J.; Lee, K.; Sekine, Y.; Reeder, J. T.; Jeang, W. J.; Aranyosi, A. J.; Lee, S. P.; Model, J. B.; Ghaffari, R.; Su, C.-J.; Leshock, J. P.; Ray, T.; Verrillo, A.; Thomas, K.; Krishnamurthi, V.; Han, S.; Kim, J.; Krishnan, S.; Hang, T.; Rogers, J. A. Battery-free, skin-interfaced microfluidic/electronic systems for simultaneous electrochemical, colorimetric, and volumetric analysis of sweat. *Sci. Adv.* **2019**, *5*, No. eaav3294.
(24) Monsalve, K.; Mazurenko, I.; Lalaoui, N.; Le Goff, A.; Holzinger, M.; Infossi, P.; Nitsche, S.; Lojou, J. Y.; Giudici-Orticoni, M. T.; Cosnier, S.; Lojou, E. A H_2/O_2 enzymatic fuel cell as a sustainable power for a wireless device. *Electrochem. Commun.* **2015**, *60*, 216−220.
(25) Zeng, Y.; Zhang, X.; Meng, Y.; Yu, M.; Yi, J.; Wu, Y.; Lu, X.; Tong, Y. Achieving Ultrahigh Energy Density and Long Durability in a Flexible Rechargeable Quasi-Solid-State Zn-MnO_2 Battery. *Adv. Mater.* **2017**, *29*, 1700274.
(26) Li, H.; Han, C.; Huang, Y.; Huang, Y.; Zhu, M.; Pei, Z.; Xue, Q.; Wang, Z.; Liu, Z.; Tang, Z.; Wang, Y.; Kang, F.; Li, B.; Zhi, C. *Energy Environ. Sci.* **2018**, *11*, 941−951.
(27) Li, H.; Liu, Z.; Liang, G.; Huang, Y.; Huang, Y.; Zhu, M.; Pei, Z.; Xue, Q.; Tang, Z.; Wang, Y.; Li, B.; Zhi, C. Waterproof and tailorable elastic rechargeable yarn zinc ion batteries by a cross-linked polyacrylamide electrolyte. *ACS Nano* **2018**, *12*, 3140−3148.
(28) Zhang, N.; Cheng, F.; Liu, J.; Wang, L.; Long, X.; Liu, X.; Chen, J. Rechargeable aqueous zinc-manganese dioxide batteries with high energy and power densities. *Nat. Commun.* **2017**, *8*, 405.
(29) Jeerapan, I.; Sempionatto, J. R.; Pavinatto, A.; You, J.- M.; Wang, J. Stretchable biofuel cells as wearable textile-based self-powered sensors. *J. Mater. Chem. A* **2016**, *4*, 18342−18353.
(30) Bandodkar, A. J.; Jeerapan, I.; Wang, J. Wearable Chemical Sensors: Present Challenges and Future Prospects. *ACS Sens.* **2016**, *1*, 464−482.
(31) Li, W.; Fang, R.; Xia, Y.; Zhang, W.; Wang, X.; Xia, X.; Tu, J. Multiscale Porous Carbon Nanomaterials for Applications in Advanced Rechargeable Batteries. *Batteries Supercaps* **2019**, *2*, 9−36.
(32) Wu, C.; Maier, J.; Yu, Y. Generalizable Synthesis of Metal-Sulfides/Carbon Hybrids with Multiscale, Hierarchically Ordered Structures as Advanced Electrodes for Lithium Storage. *Adv. Mater.* **2016**, *28*, 174−180.
(33) Qiu, W.; Li, Y.; You, A.; Zhang, Z.; Li, G.; Lu, X.; Tong, Y. High-performance flexible quasi-solid-state Zn-MnO_2 battery based on MnO_2 nanorod arrays coated 3D porous nitrogen-doped carbon cloth. *J. Mater. Chem. A* **2017**, *5*, 14838−14846.
(34) Xu, C.; Li, B.; Du, H.; Kang, F. Energetic zinc ion chemistry: the rechargeable zinc ion battery. *Angew. Chem., Int. Ed.* **2012**, *51*, 933−935.
(35) Alfaruqi, M. H.; Mathew, V.; Gim, J.; Kim, S.; Song, J.; Baboo, J. P.; Choi, S. H.; Kim, J. *Chem. Mater.* **2015**, *27*, 3609−3620.
(36) Pan, H.; Shao, Y.; Yan, P.; Cheng, Y.; Han, K. S.; Nie, Z.; Wang, C.; Yang, J.; Li, X.; Bhattacharya, P.; Mueller, K. T.; Liu, J. Reversible aqueous zinc/manganese oxide energy storage from conversion reactions. *Nature Energy* **2016**, *1*, 16039.

DOI: 10.1021/acssensors.9b00891
ACS Sens. 2019, 4, 1925−1933

(37) Zhang, N.; Cheng, F.; Liu, J.; Wang, L.; Long, X.; Liu, X.; Li, F.; Chen, J. Rechargeable aqueous zinc-manganese dioxide batteries with high energy and power densities. *Nat. Commun.* **2017**, *8*, 405.
(38) Xu, J.; Chen, Y.; Dai, L. Efficiently photo-charging lithium-ion battery by perovskite solar cell. *Nat. Commun.* **2015**, *6*, 8103.

DOI: 10.1021/acssensors.9b00891
ACS Sens. 2019, 4, 1925−1933